An On-Orbit Experiment for Dynamics and Control of Large Structures

Harry J. Buchanan,* Richard W. Schock,† and Henry B. Waites‡
NASA Marshall Space Flight Center, Alabama

A large solar array test article is planned for flight in 1984. This paper discusses the on-orbit dynamic testing planned for this flight as well as the design of a proposed experiment using this same structure in conjunction with a two- or three-axis gimbal system to demonstrate control techniques applicable to large systems. Experiment objectives, hardware, software, and planned operations are detailed.

Introduction

FOR several years, considerable thought and effort have been expended by the controls community in search of solutions to the control problems posed by large space systems. Many potential problems have been outlined, such as: 1) the need to cope with the control system frequency embedded within the densely packed modal frequencies of the large, lightweight structure; 2) the need to provide active damping for many of the structure's low-frequency modes; 3) the need to distribute sensors and actuators over a large system; and 4) the need to isolate precision-pointing elements from disturbances originating in other portions of the structure. The proposed control experiment addresses these objectives, as will be discussed.

To be technically viable, an experiment must address a set of relevant objectives, such as those listed above. To be practical, it must also be economical, compared to building and flying an actual large system. One way to avoid high cost is to combine existing flight-qualified equipment into an experiment that can be flown and recovered with NASA's Space Transportation System. In this way, hardware cost is minimized and only the cost of items peculiar to the experiment (for example, special software) is incurred. Thus, we have in the Solar Array Flight Experiment (SAFE) structure, a test specimen, already developed and flight-qualified, which embodies the salient characteristics of a typical large space structure. This paper proposes that after this structure has flown initially, it is coupled with an existing experiment pointing system mentioned in the abstract. The combination would then constitute an affordable set of flight hardware.

NASA has built and will fly a solar array test article aboard a Shuttle mission. Called the Solar Array Flight Experiment (SAFE 1), it consists of a coilable longeron mast which deploys a large solar array blanket. This structure exhibits the basic characteristics of large space structures as follows.

1) Large size (31.5×6.2 m) Kapton blanket.

2) A mechanically complex extendable/retractable ABLE mast.

3) Many low-frequency modes closely packed (four modes below 0.1 Hz).

4) Many nonplanar low-frequency modes.

5) Inability to test structural dynamics of structure accurately in earth's atmosphere and 1 g.

For these reasons it seemed a viable structure for an experiment. Multipurpose control actuator systems are being developed for use as experiment pointing systems. One of these, Annular Suspension Pointing (ASP) Gimbal System (AGS) has a three-axis torque-controlled gimbal system, a digital flight computer, and sets of accelerometers and rate gyros. Another pointing mount candidate is the European Instrument Pointing System, which also has a three-axis torquer-controlled gimbal system, attitude reference sensors, and accelerometers, but which probably needs an extra microprocessor to process the control equations. The two-axis CIRRIS-82 Pointing Control System is another possible candidate for use in the experiment. While the CIRRIS-82 has only a two-axis pointing mount, the low cost makes the system very attractive. These units could support the experiment by supplying most off the attitude control system hardware required. The utilization of these two elements (see Fig. 1) is the cornerstone of the planned experiment. While this paper has as its chief topic the design of a flight control experiment, two related activities will also be discussed at some length, 1) a ground verification facility which could demonstrate the flight experiment concept, and 2) the on-orbit dynamic testing planned for the structural test article to be used as part of this experiment.

In the past, the control engineer could specify structural constraints so that the dynamics and control interactions were minimal. The structural constraints were specified after many iterations in the system modeling and the control synthesis and analysis. In addition, there was considerable hardware closed-loop analysis to verify the models used in the analytic simulations for previous Marshall Space Flight Center (MSFC) flight systems. Minimizing dynamics and control interaction and hardware closed-loop testing were and still are an integral part in assuring success in any flight system.

Because of the large space structure characteristics, the control engineer no longer has the option of specifying structural constraints. This implies that control design must take into account system dynamics inside the controller bandwidth. System modes within the controller bandwidth have a penchant for dynamics and control interactions. If the control design is properly done, the controller should add damping, if possible, to the vibrational modes within the controller bandwidth. Since there are modes within the controller bandwidth, the control synthesis is very much dependent upon the accuracies of the system modeling. Inaccuracies in the system model not only could lead to a performance degradation, but also to system instabilities. It is imperative to have not only good system models and a robust controller, but also to have closed-loop ground and flight tests.

Received Feb. 25, 1982; revision received March 19, 1984.

*Chief, Dynamics and Trajectory Analysis Branch, Systems Dynamics Laboratory.

†Chief, Environmental Analysis Branch, Systems Dynamics Laboratory.

‡Aerospace Engineer, Pointing Control Systems Branch, Systems Dynamics Laboratory.

Because of these new requirements, it was decided to postulate a large orbital configuration and use it to ferret out the primary issues related to modeling, control analysis and synthesis, ground testing, and flight experiments. To accomplish this, the following tasks were defined for this postulated design problem:

1) Identification of system level requirements and constraints.

2) Formulation of the necessary math models, synthesis of the control system logic, and performance simulations to determine performance.

3) Establishment of a preliminary orbital experiment concept.

4) Establishment of a proof of concept (POC) ground demonstration test concept.

5) Carrying out of detailed analysis of both orbital and ground test designs comparing system performance.

Several interesting iterations transpired before a final system configuration was established. The initial configuration, which is shown in Fig. 2, consisted of the deployable beam structures, the Skylab, and the Shuttle. The Shuttle was to be equipped with control moment gyros and, with the Skylab control system, could provide centralized, distributed, and decentralized control configurations. Since the Shuttle was not operational in time to reboost Skylab to a longer decaying orbit, this configuration was no longer viable. The next configuration, shown in Fig. 3, consisted of an Orbiter and a deployable antenna which was end-mounted to a pointing mount. Sensor and effectors were to be located at the antenna hub so that the various control configurations could be implemented. Because of the program costs and scheduling, this configuration had to be dropped. In Fig. 4, the third alternate for the flight experiment is shown. It consists of the solar array, a pointing mount, reaction wheels, strain gages, rate gyros and accelerometers. The flight system provides not only the previous control configurations, but also the possibility of figure control with the strain gages in the closed loop. However, due to the cost of the additional control software and the hardware interfaces for the strain gages and the reaction wheels, this flight configuration had to be eliminated. The final configuration, which is shown in Fig. 1, can demonstrate centralized control, distributed sensor control, and disturbance isolation control. While the configuration cannot implement the distributed control and the decentralized control concepts, it does provide a first venture into the control of large space structures under the present budgetary constraints.

Ground Test Verification

One of the major objectives of this effort was to design and determine the cost of a ground test facility and an experiment which could verify dynamics and control system concepts being considered for future large space structure applications. The experiment requires sufficient fidelity to ensure reasonably successful on-orbit operation; the ground facility should be sufficiently vesatile to test a myriad of flight experiments or their suitable hardware models. A schematic for the MSFC ground test facility showing the various components and their interfaces is pictured in Fig. 5.

This facility is nearing completion and will have the capability to test a range of systems, such as the ones shown in Figs. 5 and 6.

Dynamic Experiment

An on-orbit dynamic test of a large space structure is planned for 1984. The SAFE 1 experiment includes systems for remotely sensing and recording the dynamics response of the array and postprocessing the data to determine solar array dynamic characteristics. Determining the dynamic characteristics of this structure during the first flight could support

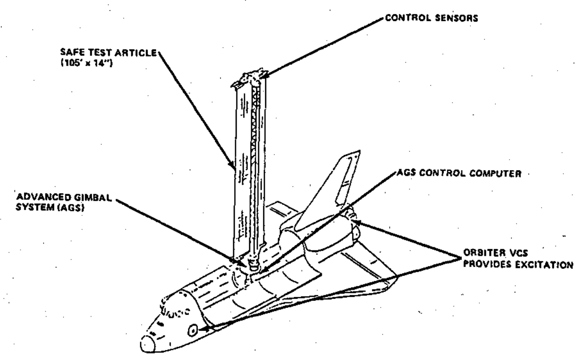

Fig. 1 Safe control experiment.

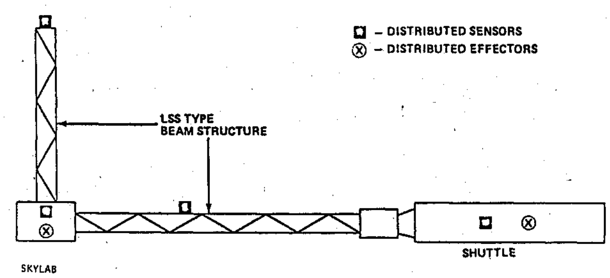

Fig. 2 First orbital experiment configuration.

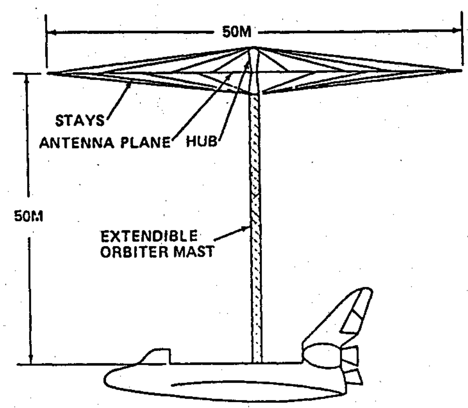

Fig. 3 Deployable antenna flight configuration.

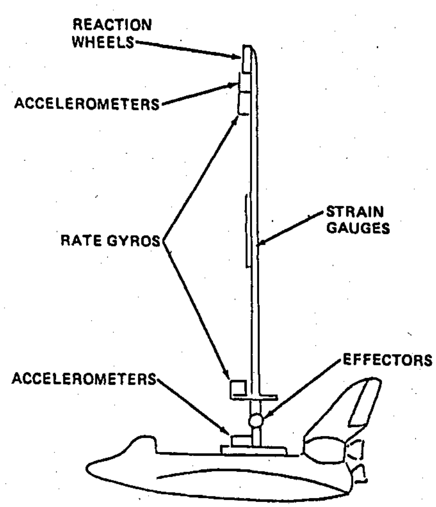

Fig. 4 Initial SAFE II flight experiment.

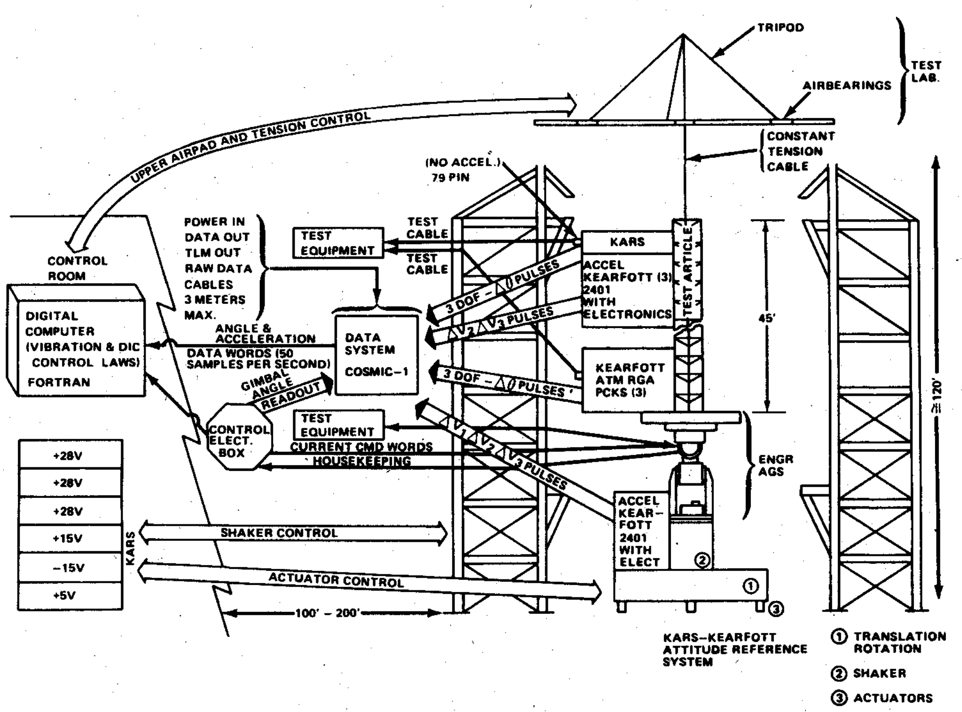

Fig. 5 Ground test configuration for SAFE II.

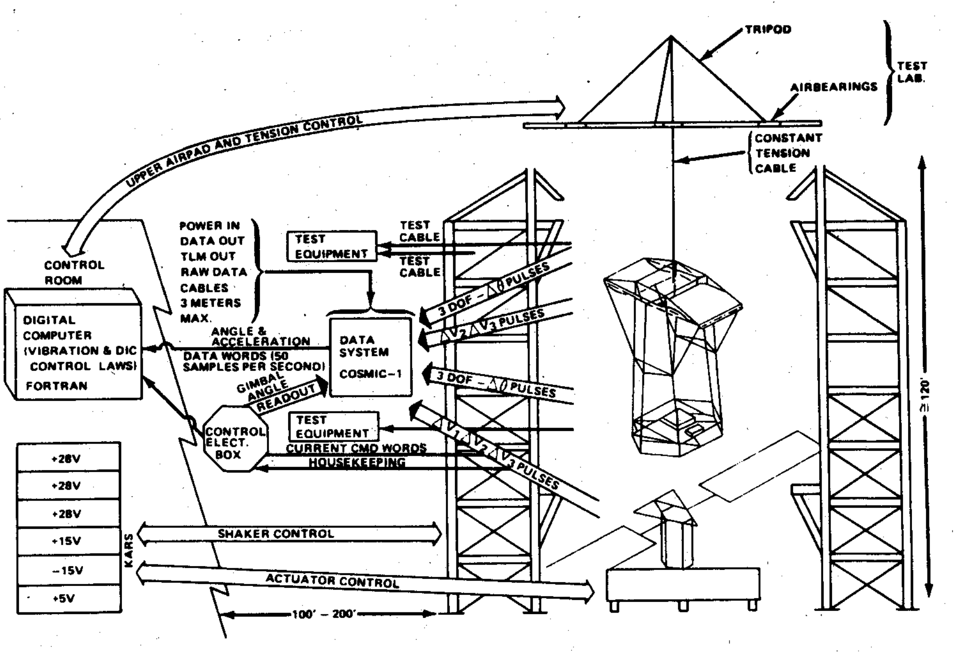

Fig. 6 DARPA model ground configuration.

development of the control experiment and aid in the interpretation of control results.

Specifically, the detailed objectives of this portion of the project are to:

1) develop and qualify for flight remote sensing systems capable of measuring solar array motions along the X and Y coordinate axes of the Space Transporation System (STS);

2) demonstrate by flight experiment the adequacy of the remote sensing system, including targets, optics, electronics, and software for measuring the dynamic motions of the SAFE Solar Array and future large space structures;

3) determine amplitudes of response, mode shapes, damping, and frequencies of the SAFE Solar Array resulting from planned motions of the STS Orbiter;

4) correlate flight responses with theoretical model results and with ground test results to determine needed refinements in analytical and test techniques.

Actually, two remote sensing systems are being planned for the first flight. The first, a photogrammetric system developed by NASA Langley Research Center, will not be discussed in this paper. The second, developed by NASA Marshall, will be discussed herein.

The remote sensor system as pictured in Fig. 7 will consist of an illuminator/receiver mounted at the base of the solar array, which will provide a light source to illuminate an array of reflective targets mounted on the solar array mast and blanket. The reflected images will be viewed by the receiver and focused on a light-sensitive detector array. Angular X, Y motion of the reflectors will be accurately sensed by the detector array; outputs proportional to angular deflections of each reflector image will be input to a microprocessor. The microprocessor contains algorithms which will convert the angular deflections to linear deflections and put out a digital data stream through a modulator to a tape recorder. The

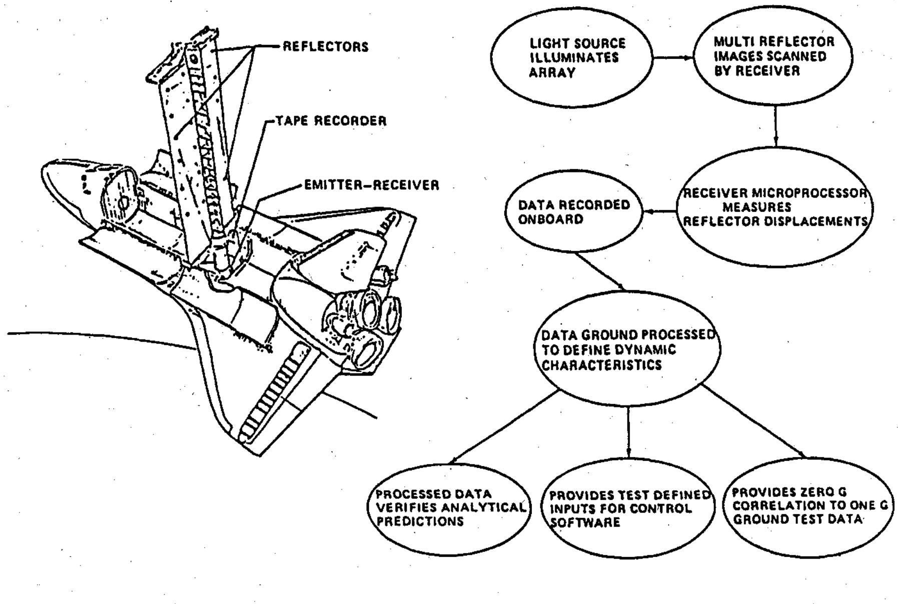

Fig. 7 SAFE dynamic experiment.

Table 1 Control gains and flexible body data

$$\begin{bmatrix} -6.15E4 & 0 & 0 & -4.16E4 & 0 & 0 \\ 0 & -3.73E4 & 0 & 0 & -4.28E4 & 0 \\ 0 & 0 & -281 & 0 & 0 & -197 \end{bmatrix}$$

Modal frequencies are
FSXY
0 0.0353 0.058 0.117 0.177 0.239 0.24 0.302 0.303 0.309
XY plane slopes at sensor and torquer are
XSEP
0.00369 0.005 −0.00217 −0.0028 0.0031 0.00292
−5.8E−6 1.76E−5 −0.0032 −1.27E−5
XZ plane slopes at sensor and torquer are
YSEP
0.0039 −2.57E−7 4.4E−7 −6.8E−7 −1.12E−6 2E−5
−0.00117 0.0074 4.3E−5 −0.00368
YZ plane slopes at sensor and torquer are
ZSEP
0.07 0.00346 0.032 0.06 −0.064 −0.05 −0.00027 −0.000376
0.04 −4E−5

[a] Gain units are n-m (rad/s) and n − m/rad; slope units are rad/m.

recorded data will be returned and on the ground processed to obtain array frequency, modal characteristics, and damping.

Excitation of the array will be accomplished by Orbiter vernier control system (VCS) firings. Dynamic analyses are in progress to determine the optimum sequence of VCS firing for obtaining maximum multimodal response without exceeding the solar array base bending moment capability. Ground tests, using a 10-m lightweight space frame, are planned as an early proof of concept demonstration. The 10-m space frame will be cantilevered vertically. A large mass will be attached to the free end to reduce the natural frequency. A ground test remote sensor system will record the motion of light-emitting diodes mounted on the structure. Accelerometers will also be installed and recorded as reference data. Remote sensing data will, in turn, be analyzed to determine response motions and structural dynamic characteristics, and will be compared to the results obtained by accelerometers in conventional dynamic evaluation methods.

Controls Experiment

SAFE Control Design Model

Table 1 depicts the SAFE modal description which was obtained by a NASA Structural Analysis (NASTRAN) finite element model. The NASTRAN physical parameters used in the attitude control design are the modal frequencies and the eigenvector slopes in the various control planes. Of importance from a control standpoint are the slope values at the location of the sensors and torque positions.[1] Table 1 shows two important factors relative to the eigenvector slopes. Since the sensor and torque (per plane) are colocated, the slopes have the same value. Colocation of the sensors and effectors gives the control design engineer a special path to assuage stability problems relative to the placement of the control elements. Also, the product of these slopes is a direct multiple of the system control gains. If the product of a a particular mode is small, then a great effector influence is necessary to control that mode and vice versa. For this experiment, the ideal location would be where the attitude sensor and torquer could exert the greatest influence, i.e., at a location of maximum slope of the modal eigenvector.[2] Because of the structural complexity, packaging, and cost, one set of sensors is located on the pointing mount and another at the experiment tip. A set of effectors also located at the experiment tip would give a colocated distributed control setup at some increase in cost.

Based upon past experience with spacecraft, a damping of ½% for each mode was selected for the control synthesis. Table 2 contains the open-loop eigenvalues obtained using the modal data in Table 1 and the ½% damping value. The second and third columns in the table are the real and imaginary value of the eigenvalues. For a high "Q" system, such as the flight experiment model, a good approximation to the structural damping is the magnitude ratio of the real to the imaginary.[3] Also, the modal frequency can be obtained by dividing the imaginary magnitude by 2π. A quick scan of Table 2 shows that the damping of each mode is ½% and the imaginary values correspond to the modal frequencies in rad/s. Once the model is specified, the control objectives can be established and the control synthesis initiated.

Control System Objectives

The objectives for the SAFE control experiment planned for the reflight, which parallel those given previously in the introduction, are to demonstrate a scheme utilizing centralized sensors and actuators, to effect the use of distributed sensor control, and to implement a technique for isolating disturbances by the use of active control. The control problem is delineated by considering the modal frequency description of a space structure which is

$$\mathfrak{F} = \{f_1, f_2, f_3, \dots\}$$

where f_i's are the structural modal frequencies

$$f_i < f_{i+1}, \qquad |f_i - f_{i+1}| < \Delta$$

and Δ depends upon the particular space structure. For previous NASA space structures, such as the Saturn V and the Skylab, the fundamental frequency, f_1, was large enough so that adequate dynamic response could be achieved by selecting a controller frequency, f_c less than f_1.

Using the same control design procedures as mentioned for Saturn V and the Skylab, the control frequency would be less than the SAFE fundamental frequency which is 0.0353 Hz. If a control frequency of $0.1 f_1$(0.00353 Hz) was selected so that the dynamic/control interaction would be minimal, then the dynamic performance with respect to disturbances and commanded inputs would suffer. Although the control system would not appreciably excite any modes, external disturbances and commanded inputs to the flight experiment would excite the vibrational modes. Since all the modes except the rigid body have ½% damping (see Table 2), this implies that the time for these modes to damp out is inversely proportional to the product of the modal damping and the modal frequency in rad/s. Control synthesis techniques which use this procedure are called gain stabilized control systems. One of the control problems addressed for the SAFE control experiment is to imbed a control frequency, f_c, in the modal description so that the system is stable and has improved dynamic response. Since the Δ_{max} for the experiment is 0.062 Hz, this constraint provides an additional challenge in the control design, i.e., to embed a control frequency, f_c, in

$$\mathfrak{F}_c = \{\bar{f}_1, \bar{f}_2, \ldots, \bar{f}_i, f_c, \bar{f}_{i+1}, \ldots\}$$

where $\bar{f}_i$'s are the structural modal frequencies of $\mathfrak{F}_c$ with

$$\bar{f}_i < \bar{f}_{i+1}, \quad \bar{f}_1 = 0.0353 \text{ Hz, and } |\bar{f}_i - \bar{f}_{i+1}| \leq 0.062 \text{ Hz}$$

Embedding a control frequency in nested modes by use of classical or optimal control techniques is a very tedious undertaking. Because of the dynamic and control interaction, the classical techniques require several iterations to accomplish this goal. Because of the large system order, the optimal control approach requires the solution of a high-order Riccati equation to obtain the control gain necessary for the imbedding tasks. In either case, the embedding of a control frequency in a group of densely spaced modes is not a trivial task.

Table 2 Open loop eigenvalues[a]

No.	Re	Im (rad/s)
1	$-0.9514000E-02$	1.9026862
2	$-0.9514000E-02$	-1.9026862
3	$-0.18212000E-02$	0.36423545
4	$-0.18212000E-02$	-0.36423545
5	$-0.55578000E-02$	1.1115461
6	$-0.55578000E-02$	-1.1115461
7	$-0.7536000E-02$	1.5071812
8	$-0.7536000E-02$	-1.5071812
9	$-0.11084200E-02$	-0.22168123
10	$-0.11084200E-02$	-0.22168123
11	$-0.97026000E-02$	1.9404957
12	$-0.97026000E-02$	-1.9404957
13	$-0.36738000E-02$	0.73475082
14	$-0.36738000E-02$	-0.73475082
15	$-0.75046000E-02$	1.5009012
16	$-0.75046000E-02$	-1.5209012
17	$-0.94828000E-02$	1.8965363
18	$-0.94828000E-02$	-1.8965363
19	0.00000000	0.00000000
20	0.00000000	0.00000000

[a] Wilkinson error measure max $\mu = 055021088E-01$ (exit).

Theoretical Control Development

Current control procedures for large flexible space vehicles employ the following techniques and theories:

1) A perturbation controller for low-authority control with optimal control for high-authority control.[4]
2) Positivity concepts which use hyperstability theory.[5-7]
3) Model reference adaptive techniques,[8,9]
4) Pole placement schemes.[10-15]
5) Various combinations of the above.

All of these techniques have merit relative to control system synthesis.

The control system approach used for this design is a closed form pole placement scheme (CFPPS). The CFPPS allows for relatively easy placement of the control system frequencies in the densely spaced nonplanar modes of large space structures. Also, the control scheme uses only output feedback which reduces software costs. In addition to the attitude control design, a disturbance isolation controller is developed to reduce the Orbiter disturbance effects transmitted to the SAFE control experiment. When a modal coordinate description of the flight experiment is used, the closed-loop pole placement controller design and the disturbance isolation controller design yield closed-form solutions. Closed-form solutions are extremely important, especially when designing sampled-data controllers.

The CFPPS allows incomplete state feedback and is formulated for the system description

$$\dot{x} = Ax + Bu \tag{1}$$

$$y = Cx \tag{2}$$

$$\dot{z} = Dz + Ey, \tag{3}$$

and

$$u = Fz \tag{4}$$

where

x:$n \times 1$ plant state vector,

u:$r \times 1$ control vector,

z:$p \times 1$ control filter states, and

y: $m \times 1$ measurement vector.

The CFPPS uses techniques for both the frequency domain and the state space analysis to synthesize control systems. Using the state space analysis, it is possible to derive a set of linear algebraic relationships so that the control gains can be obtained by a matrix inverse. Not only does the pole placement scheme have a closed-form solution but the order of the algebraic relationship can be equal to the minimum of effectors or the number of the sensors. This low-order closed-form solution greatly enhances control system synthesis.[16] A brief outline for the control techniques is as follows.

First calculate the characteristic polynomial of Eqs. (1-4) which is

$$\Delta(\lambda) = |\lambda I_n - A|\,|\lambda I_P - D|\,|I_p - P(\lambda)F| \tag{5a}$$

$$= |\lambda I_n - A|\,|\lambda I_P - D|\,|I_r - FP(\lambda)| \tag{5b}$$

where

$$P(\lambda) = (\lambda I_P - D)^{-1} EC(\lambda I_n - A)^{-1} B \tag{6}$$

and

F:$r \times p$ unknown control gain matrix.

If $\Delta(\lambda_i)$ was zero, then λ_i would be a characteristic root of Eq. (5). To enforce this condition upon Eq. (5), find an F such that either the jth row of

$$|I_p - P(\lambda_i)F|_{j^*} = 0 \quad \text{or} \tag{7a}$$

$$|Ir - FP(\lambda_i)|_{j^*} = 0 \tag{7b}$$

This procedure is repeated for as many desired λ_i's up to i equal to either r or P; the control matrix F is found by solving the resultant equations obtaiend through Eq. (7) for the distinct eigenvalues.[16] If repeated eigenvalues are desired, then

$$\frac{d^s}{d\lambda^s}\left[\{\,|[I_P - P(\lambda)F]|\,\}\Big|_{\lambda=\lambda_i}\right]_{j^*} = 0 \tag{8a}$$

or

$$\frac{d^s}{d\lambda^s}\left[\{\,|[I_r - FP(\lambda)F]|\,\}\Big|_{\lambda=\lambda_i}\right]_{j^*} = 0 \tag{8b}$$

yields the necessary equations for λ_i to be a closed-loop eigenvalue of order s in Eq. (5).

The sampled-data closed-loop pole placement is very similar to the pole placement for a continuous controller except that the plant Eqs. (1) and (2) must be discretized. Assuming that the control signal u is transmitted through a zero-order-hold, the discrete system for Eq. (1) is

$$x[(i+1)T_s] = \exp(AT_s)x[iT_s] + \int_0^{T_s} \exp(A\delta)\,d\delta Bu(iT_s)$$

where T_s is the sample rate. If the plant equations are in modal coordinates, then the A matrix in Eq. (1) for a proportional-deviation (PD) controller is

$$A = \begin{bmatrix} A_1 & 0_1 & \dots & 0_1 \\ 0 & A_2 & \dots & 0_1 \\ \cdot & \cdot & \dots & \cdot \\ \cdot & \cdot & \dots & \cdot \\ \cdot & \cdot & \dots & \cdot \\ 0_1 & 0_1 & & A_t \end{bmatrix} \tag{9}$$

where

$$0_1 = \begin{bmatrix} 0 & 0 \\ 0 & 0 \end{bmatrix}, \quad A_1 = \begin{bmatrix} 0 & 1 \\ 0 & 0 \end{bmatrix},$$

and

$$A_i = \begin{bmatrix} 0 & 1 \\ -\omega_i^2 & -2\zeta_i\omega_i \end{bmatrix}$$

for $1 < 1 \leq t = n/2$, provided there is only one rigid body mode. If there is more than one rigid body mode, the matrix A_1 is expanded to encompass them. It is clear that

$$\exp(AT_s) = \begin{bmatrix} \exp(A_1T_s) & 0_1 & \dots & 0_1 \\ 0_1 & \exp(A_2T_s) & \dots & 0_1 \\ \cdot & \cdot & \dots & \cdot \\ \cdot & \cdot & \dots & \cdot \\ 0_1 & 0_1 & \dots & \exp(A_tT_s) \end{bmatrix} \tag{10}$$

and this yields for the individual 2×2 blocks

$$\exp(A_1T_s) = \begin{bmatrix} 1 & T_s \\ 0 & 1 \end{bmatrix} \tag{11}$$

and

$$\exp(A_iT_s) = \frac{\exp(\sigma_iT_s)}{\Omega_i} \times \begin{bmatrix} -\sigma_i\sin\Omega_iT_s + \Omega_i\cos\Omega_iT_s & \sin\Omega_iT_s \\ -\omega_i^2\sin\Omega_iT_s & -\zeta_i\omega_i\sin\Omega_iT_s + \Omega_i\cos\Omega_iT_s \end{bmatrix} \tag{12}$$

for $1 < 1 \leq t$. The second term in Eq. (9) is computed in a very similar manner. Integrating the 2×2 rigid body block yields

$$\int_0^{T_s}\begin{bmatrix} 1 & \delta \\ 0 & 1 \end{bmatrix} d\delta = \begin{bmatrix} T_s & T_s^2/2 \\ 0 & T_s \end{bmatrix} \tag{13}$$

and the ith 2×2 flexible body block gives

$$\int_0^{T_s}\exp(A_i\delta)\,d\delta = -A_i^{-1}[I - \exp(A_iT_s)] \tag{14}$$

for $1 < 1 \leq t$. This completes a closed-form solution for the z transform of Eq. (1). Using these results, the continuous plant

$$\dot{x} = Ax + Bu \tag{15}$$

and

$$y = Cx \tag{16}$$

is discretized which yields

$$x(i+1) = A_Dx(i) + B_Du(i) \tag{17}$$

and

$$y(i) = Cx(i) \tag{18}$$

where the sample time T_s has been dropped. The control filters and control gains for Eqs. (17) and (18) are

$$z(i+1) = Dx(i) + Ey(i) \tag{19}$$

and

$$u(i) = Fz(i) \tag{20}$$

The sampled-data CFPPS follows in exactly the same way as the continuous schemes and as such will not be delineated. As can be seen, these pole placement schemes yield a set of linear equations and as a result can be solved in closed form. When model coordinates are used, the z transform of the plant can also be calculated in a closed form. This is an ideal situation when considering a large number of modes for a control design.

The reduction of Orbiter disturbance effects transmitted to the flight experiment is the purose of the disturbance isolation controller (DIC). The DIC uses an observer which does not require direct measurement of the plant inputs to obtain estimates of the plant states and the rate of the plant states. The state and rate of the state information is used to design a contoller which isolates disturbances from specified segments of the plant; for the flight experiment, this segment is the solar array. The DIC development for the SAFE experiment is delineated in Ref. 17; therefore, the DIC design procedure will not be repeated.

Table 3 Closed loop eigenvalues for the X-Y plane 0.271 Hz controller[a]

No.	Re	Im (rad/s)
1	−1.7018800	1.7018800
2	−1.7018800	−1.7018800
3	−0.36767912E−03	0.11952021
4	−0.36767912E−03	−0.11952021
5	−0.18158004E−02	0.35028553
6	−0.18158004E−02	−0.35028553
7	−0.66412599E−02	0.67067104
8	−0.66412599E−02	−0.67067104
9	−0.17434451E−01	1.0100375
10	−0.17434451E−01	1.0100375
11	−0.27586214E−01	1.4033997
12	−0.27586214E−01	1.4033997
13	−0.36294097E−01	1.7986753
14	−0.36294097E−01	1.7986753
15	−0.97026376E−02	1.9404953
16	−0.97026376E−02	1.9404953
17	−0.94828048E−02	1.8965365
18	−0.94828048E−02	1.8965365
19	−0.75360003E−02	1.5071811
20	−0.75360003E−02	1.5071811

[a] Wilkinson error measure max $\mu = 0.70997645E-01$ (exit).

Table 4 Closed loop eigenvalues for the X-Z plane 0.271 Hz controller[a]

No.	Re	Im (rad/s)
1	−1.7018800	1.7018800
2	−1.7018800	1.7018800
3	−0.98310471E−02	1.9318620
4	−0.98310471E−02	1.9318620
5	−0.95141999E−02	1.9028160
6	−0.95141999E−02	1.9028160
7	−0.93774758E−02	1.5154759
8	−0.93774758E−02	1.5154759
9	−0.75047067E−02	1.5009023
10	−0.75047067E−02	1.5009023
11	−0.55578073E−02	1.1115461
12	−0.55578073E−02	1.1115461
13	−0.88661918E−01	0.55415215
14	−0.88661918E−01	0.55415215
15	−0.36738118E−02	0.73475083
16	−0.36738118E−02	0.73475083
17	−0.11084200E−02	0.22168123
18	−0.11084200E−02	0.22168123
19	−0.18212000E−02	−0.36423545
20	−0.18212000E−02	−0.36423545

[a] Wilkinson error measure max $\mu = 0.79706929E-01$ (exit).

The attitude control frequency selection of 0.271 Hz was based upon a number of factors, system stability, attitude and attitude rate performance, and vibration suppression. Even though these factors are interrelated, they will be analyzed as separate entities wherever possible. This analysis method provides a special insight into the pole placement control synthesis.

One of the first constraints in control design is ensuring the stability of the closed-loop system. Since stability cannot be assured by a finite number of pole placements in a continuum, the control frequency is chosen and the sensor/effector pair are colocated so that the SAFE model is stable. For the 0.271-Hz control frequency, the system model is stable. The stability was determined by the system closed-loop eigenvalues. The SAFE closed-loop eigenvalues per plane are contained in Tables 3-5. The second and third columns of each table are the real and imaginary values of these eigenvalues. The second column of all the eigenvalues is negative, which is the desired characterisic for stability.

Another important factor in control design is the control system performance. The control system performance was specified by the placement of the rigid body poles from the origin to the pole position of $-1.7 \pm j\,1.7$. This is equivalent to setting the control frequency f_c equal to 0.271 Hz with a damping value of 0.707. If the system model was a rigid body, then the attitude and attitude rate performance at the experiment base would be assured. As long as the system is stable, the higher the control frequency, the better the system performance, but limits are imposed by the required torques, torquer dynamics, sensor dynamics, control computer timing cycles, and noise. These limits are tradeoffs which the control engineer must consider while trying to improve system performance, and have not been addressed in this paper.

One of the most interesting aspects of the control design was the selection of a control frequency which has the capability of vibration suppression. For a control frequency of 0.271 Hz, Table 1 shows that there are at least six vibrational modes inside the controller bandwidth. The designer might think intuitively that the controller would add damping and possibly separate these modes in frequency because the modes are within the controller bandwidth. This is not the case for this control design.

Examining the X-P plane closed loop eigenvalues in Table 3 shows that the modal damping at 0.055, 0.1, 0.16, and 0.28 Hz has increased because of the controller. The modal

Table 5 Closed loop eigenvalues for the X-Y plane 0.271 Hz controller[a]

No.	Re	Im (rad/s)
1	−1.7018800	1.7018800
2	−1.7018800	−1.7018800
3	−0.16367685E−01	0.94628904
4	−0.16367685E−01	−0.94628904
5	−0.87177537E−02	0.53745726
6	−0.87177537E−02	−0.53745726
7	−0.20599652E−02	0.31737091
8	−0.20599652E−02	−0.31737091
9	−0.11063901E−02	0.22130570
10	−0.11063901E−02	−0.22130570
11	−0.22578067E−01	1.4008753
12	−0.22578067E−01	−1.4008753
13	−0.26713447E−01	1.8342341
14	−0.26713447E−01	−1.8342341
15	−0.97026026E−02	1.9404957
16	−0.97026026E−02	−1.9404957
17	−0.94828195E−02	1.8965369
18	−0.94828195E−02	−1.8965369
19	−0.75360013E−02	1.5071810
20	−0.75360013E−02	−1.5071810

[a] Wilkinson error measure $\mu = 0.55021088E-01$ (exit).

damping at 0.238, 0.302, and 0.308 Hz has the sample damping as in the open-loop condition. The no-damping change is expected for the 0.302 and the 0.308 Hz modes but not for the 0.238 Hz mode. Since the 0.238 Hz mode is within the controller bandwidth, the control system should add damping to this mode. No damping is added because of the slope magnitude at the sensor/effector location. The modal slope magnitude for the 0.238 Hz mode is $5.8 \cdot 10^{-6}$ rad/m which is an order of magnitude smaller than the modes in which damping was added. As mentioned in the section discussing the SAFE control design model, the slope magnitude influences the amount of control which can be exerted upon this mode.

Table 4 shows that the controller added damping to the 0.0875, 0.1769, and 0.242 Hz modes. The controller did not affect the damping of the 0.353, 0.058, 0.1169, and 0.238 Hz modes. The unaffected modes had slope magnitudes at the sensor/effector location which were at least an order of

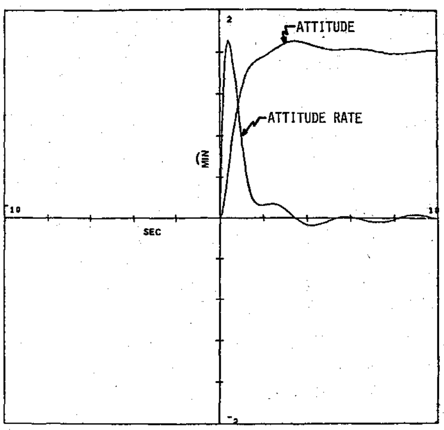

Fig. 8 *X-Y* **plane attitude and attitude rate responses to a step input for a 0.271 Hz controller.**

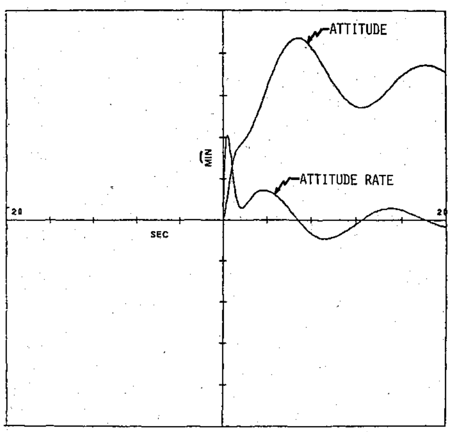

Fig. 9 *X-Z* **plane attitude and attitude rate responses to a step input for a 0.271 Hz controller.**

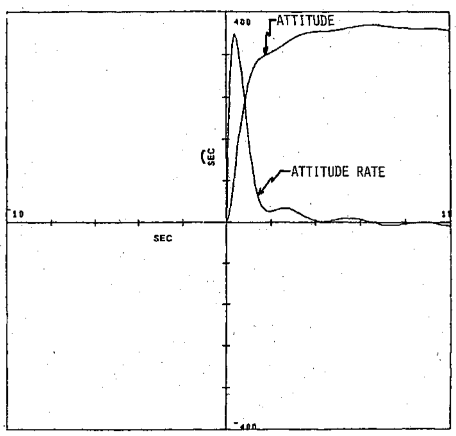

Fig. 10 *Y-Z* **plane attitude and attitude rate responses to a step input for a 0.271 Hz controller.**

magnitude smaller than the affected modes. This would imply that there is a correlation between modal slope magnitudes and controller influence as previously stated in the model description section.

Likewise, in Table 5, the closed-loop eigenvalues for the *Y-Z* plane exhibit a similar phenomenon. The controller added damping to the 0.085, 0.149, 0.2229, and 0.292 Hz modes, but added little or no damping to the 0.352, 0.0505, and 0.239 Hz modes. The modal slope magnitudes for the unaffected modes in the *Y-Z* plane are about the same magnitude as the affected modes in the *X-Y* and *X-Z* plane. All the modes in the *Y-Z* plane, however, did not have an increase in damping. The reason for this apparent anomaly is the modal slope magnitudes relative to the rigid body modal slope. The *Y-Z* plane modal slope magnitudes for the unaffected modes are an order of magnitude less than the affected modes relative to the rigid body slopes (see Table 1). Thus, if the slope magnitudes at the sensor and torquer for a particular mode are smaller relative to other modes inside the controller bandwidth, the control authority is also small. Therefore, very little, if any, damping will be added to this mode by the controller.

The closed-loop eigenvalues do not indicate complete reason for the control system performance. The time responses are necessary so that the attitude and attitude rate performance can be examined. Figures 8-10 show the time responses to a step disturbance for the 0.271 Hz controller in the *X-Y*, *X-Z*, and *Y-Z* planes. Figure 8, which consists of the *X-Y* plane attitude and attitude rate at the pointing mount, shows response time of approximately 2 s with very little overshoot. The oscillation is the 0.055 Hz mode, it is ringing out at ½% damping. While the 0.055 Hz mode is within the controller bandwidth, the controller does not cause the excitation because the control authority is negligible (see Table 1 for slope of 0.055 Hz mode). The *X-Z* plane attitude and attitude rate at the SAFE base is shown in Fig. 9. The rigid body rise time is approximately 2 s, but the 0.058 Hz mode has a response magnitude nearly equal to that of the rigid body. The large vibrational magnitude relative to the rigid body mode occurs because the modal slope at the disturbance application point is nearly the same as the slope of the rigid body at the same point. This mode also rings out at ½% damping. The *Y-Z* plane attitude and attitude rate, shown in Fig. 10, evidences very little modal vibration because of the disturbance. Therefore, most of the attitude response is rigid body motion.

Conclusion

At least one mode in each plane which is inside the bandwidth of the controller is unaffected by the control gains. The results show that the amount of control authority is dependent upon the product of the slope at the sensor and at the effector and, consequently, upon the placement of the sensors and effectors. Similarly, if the effector has little control authority, then the mode is not excited by the control system. These conclusions are borne out in the previous analysis of the closed-loop eigenvalues and time responses.*

Summary

Flight testing of control concepts for large systems is needed prior to initiating a major program. Economics seem to dictate that these requirements be filled by utilizing existing flight equipment. Details of one such experiment have been presented with regard to objectives and implementation. This experiment addresses several of the problems associated with large space platforms, notably, the damping of large low-frequency appendates; isolation of experiments from disturbances arising in another portion of the platform; and stabilization using a controller frequency which lies within the structure's modal frequency range. It should contribute measurably to the technology required for multipurpose space platforms supporting science, industrialization, and manned operations.

References

[1] Blakelock, J.H., *Automatic Control of Aircraft and Missiles,* John Wiley and Sons, Inc., New York, 1965, pp. 249-267.

[2] Likins, P.W., "A Study of Attitude Control Concepts for Precision-Pointing Nonrigid Spacecraft," NASA CR-2619, Oct. 1975.

[3] Mason, S.J., and Zimmerman, H.J., *Electric Circuit Signals and Systems,* John Wiley and Sons, Inc., New York, 1960.

[4]Lyon, M.G., Aubrun, J.N., Margulies, G., Gupta, N.K., et al., "ACOSS Three (Active Control of Space Structure) Phase 1," Rome Air Development Center, TR-80-131, May 1980.

[5]Benhabib, R.J., Iwens, R.P., and Jackson, R.L., "Stability of Distributed Control for Large Flexible Structures Using Positivity Concepts," AIAA Paper 79-1780, Boulder, Colo., Aug. 6-8, 1979.

[6]Benhabib, R.J., Iwens, R.P., and Jackson, R.L., "A Unified Approach to the Design of Large Space Structure Control Systems," Joint Automatic Control Conference, 1980.

[7]Iwens, R.P., "Challenges in Stable and Robust Control Systems Design for Large Space Structures," IEEE Conference on Decision and Control, Albuquerque, N. Mex., Dec. 10-12, 1980.

[8]Benhabib, R.J., Iwens, R.P., and Jackson, R.L., "Active Vibration Control of a Flat Rate Using Model Reference Adaptive Techniques," *Second Virginia Polytechnic Institute Symposium on Dynamics and Control of Large Flexible Spacecraft,* June 21-23, 1979.

[9]Benhabib, R.J., Iwens, R.P., and Jackson, R.L., "Adaptive Control for Large Space Structures," *18th IEEE Conference on Decision and Control,* Fort Lauderdale, Fla., Dec. 12-14, 1979.

[10]Davison, E.J., "On Pole Assignment in Linear Systems With Incomplete State Feedback," *IEEE Transations on Automatic Control,* Vol. AC-15, June 1970, pp. 348-351.

[11]Davison, E.J. and Chatterjee, R., "A Note on Pole Assignment in Linear Systems with Incomplete State Feedback," *IEEE Transactions on Automatic Control,* Vol. AC-16, Feb. 1971, pp. 98-99.

[12]Davison, E.J., and Chow, S.G., "An Algorithm for the Assignment of Closed-Loop Poles Using Output Feedback in Large Linear Multivariable Systems," *IEEE Transactions on Automatic Control,* Vol. AC-18, Feb. 1973, pp. 74-75.

[13]Davison, E.J. and Wang, S., "Properties of Linear Time-Invariant Multivariable Systems Subject to Arbitrary Output and State Feedback," *IEEE Transactions on Automatic Control,* Vol. AC-18, No. 1, Feb. 1973.

[14]Davison, E.J. and Wang, S., "On Pole Assignment in Linear Multivariable Systems Using Output Feedback," *IEEE Transactions on Automatic Control,* Vol. AC-20, Aug. 1975, pp. 516-518.

[15]Kimura, H., "A Further Result on the Problem of Pole Assignment by Output Feedback," *IEEE Transactions on Automatic Control,* Vol. 3, AC-22, June 1977, pp. 458-463.

[16]Waites, H.B., "An Observer for a Deployable Antenna," AIAA Paper 81-0453, Feb. 1981.

[17]Waites, H.B., "Disturbance Isolation Control for the Safe Flight Experiment," *Large Space Systems Technology 1981 Third Annual Technical Review,* Langley Research Center, Hampton, Va., Nov. 16-19, 1981, pp. 345-362.